Importance of C*−H Based Modes and Large Amplitude Motion Effects in Vibrational Circular Dichroism Spectra: The Case of the Chiral Adduct of Dimethyl Fumarate and Anthracene

ARTICLE *in* THE JOURNAL OF PHYSICAL CHEMISTRY A · MAY 2014

Impact Factor: 2.69 · DOI: 10.1021/jp502544v · Source: PubMed

6 AUTHORS, INCLUDING:

Giovanna Longhi
Università degli Studi di Brescia
100 PUBLICATIONS **965** CITATIONS
SEE PROFILE

Susan Lepri
Università degli Studi di Perugia
10 PUBLICATIONS **38** CITATIONS
SEE PROFILE

Renzo Ruzziconi
Università degli Studi di Perugia
113 PUBLICATIONS **1,189** CITATIONS
SEE PROFILE

THE JOURNAL OF PHYSICAL CHEMISTRY A

Article

pubs.acs.org/JPCA

Importance of C*−H Based Modes and Large Amplitude Motion Effects in Vibrational Circular Dichroism Spectra: The Case of the Chiral Adduct of Dimethyl Fumarate and Anthracene

Marco Passarello,[†,⊥] Sergio Abbate,*[,†,‡] Giovanna Longhi,[†,‡] Susan Lepri,[§] Renzo Ruzziconi,*[,§] and V. P. Nicu*[,∥]

[†]Dipartimento di Medicina Molecolare e Traslazionale, Università di Brescia, Viale Europa 11, 25123 Brescia, Italy

[‡]CNISM Consorzio Nazionale Interuniversitario per le Scienze Fisiche della Materia, Via della Vasca Navale, 84, 00146 Roma, Italy

[§]Dipartimento di Chimica, Biologia e Biotecnologie, Università di Perugia, via Elce di Sotto 8, 06100 Perugia, Italy

[∥]Theoretical Chemistry, Vrjie Universiteit Amsterdam, De Boelelaan 1083, 1081 HV Amsterdam, The Netherlands

Supporting Information

ABSTRACT: The role played by the C*−H based modes (C* being the chiral carbon atom) and the large amplitude motions in the vibrational absorption (VA) and vibrational circular dichroism (VCD) spectra is investigated. The example of an adduct of dimethyl fumarate and anthracene, i.e., dimethyl-(+)-(11*R*,12*R*)-9,10-dihydro-9,10-ethanoanthracene-11,12-dicarboxylate, and two deuterated isotopomers thereof specially synthesized for this goal, are considered. By comparing the experimental and DFT calculated spectra of the undeuterated and deuterated species, we demonstrate that (1) the C*−H bending, rocking, and stretching modes in the VA and VCD spectra are clearly identified in well defined spectroscopic features; (2) significant information about the conformer distribution is gathered by analyzing the VA and VCD data of both the fingerprint and the C−H stretching regions, with particular attention paid to the band shape data. Effects related to the large amplitude motions of the two methoxy moieties have been simulated by performing linear transit (LT) calculations, which consists of varying systematically the relative positions of the two methoxy moieties and calculating VCD spectra for the partially optimized structures obtained in this way. The LT method allows one to improve the quality of calculated spectra, as compared to experimental results, especially in regard to relative intensities and bandwidths.

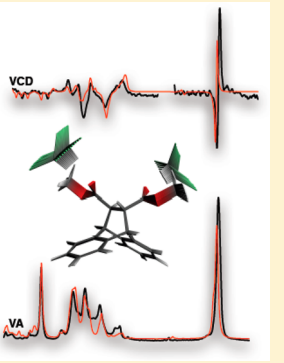

1. INTRODUCTION

Molecular chiral systems in most cases are devoid of symmetry, though it is known that, to be chiral, an object should "only" miss any of the following symmetry elements: mirror plane, inversion center, S_n planes.[1,2] This has made C_n-symmetry endowed molecules, like, e.g., allene-based molecules, biphenyls, binaphthyls, and helicene-based systems, particularly attractive in studying chiroptical properties like optical rotation (OR) or electronic circular dichroism (ECD).[3] In vibrational circular dichroism (VCD) spectra[3−16] many features are present and symmetry could help classify different kinds of bands as associated with different kinds of phenomena. Not only is this particularly true for the mid-IR region, where we recall the example of (*S*)-(1,3)-dimethyl allene[17] and (1,2)-*trans*-dideuterio-oxirane,[18] but also the CH-stretching region (even in the NIR region) was investigated in the past for these and analogous systems.[18−20]

To combine the virtues of symmetry and deuteration (as recalled in refs 17−20 above), in this work we consider as our case of study the dimethyl (+)-(11*R*,12*R*)-9,10-dihydro-9,10-ethanoanthracene-11,12-dicarboxylate, its enantiomer dimethyl (−)-(11*S*,12*S*)-9,10-dihydro-9,10-ethanoanthracene-11,12-dicarboxylate and two specifically deuterated isotopomers derived from them. (As shown in Scheme 1, the considered example molecules will be referred hereafter as (*R*,*R*)-**1**, (*R*,*R*)-**1**-d_6 and (*R*,*R*)-**1**-d_{16}, (*S*,*S*)-**1**, (*S*,*S*)-**1**-d_6, and (*S*,*S*)-**1**-d_{16}, respectively.)

The extensive use of deuteration (which localizes or, better said, restricts the delocalization of the modes) together with the C_2 symmetry of the chemical structure for the chosen molecular systems should allow us to better understand the nature of the numerous monosignate and bisignate features in the vibrational

Scheme 1. Chemical Structures of the Compounds (*R*,*R*)-1, (*R*,*R*)-1-d_6, and (*R*,*R*)-1-d_{16} and Their Enantiomers (*S*,*S*)-1, (*S*,*S*)-1-d_6, and (*S*,*S*)-1-d_{16}.

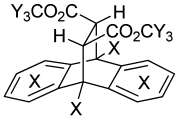

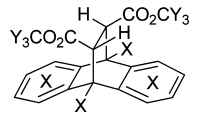

Received: March 13, 2014
Revised: May 19, 2014

   dx.doi.org/10.1021/jp502544v | *J. Phys. Chem. A* XXXX, XXX, XXX−XXX

Scheme 2. Synthesis of Compounds (*R,R*)-1, (*R,R*)-1-d_6, and (*R,R*)-1-d_{16} and Their Respective Enantiomers (*S,S*)-1, (*S,S*)-1-d_6, and (*S,S*)-1-d_{16}

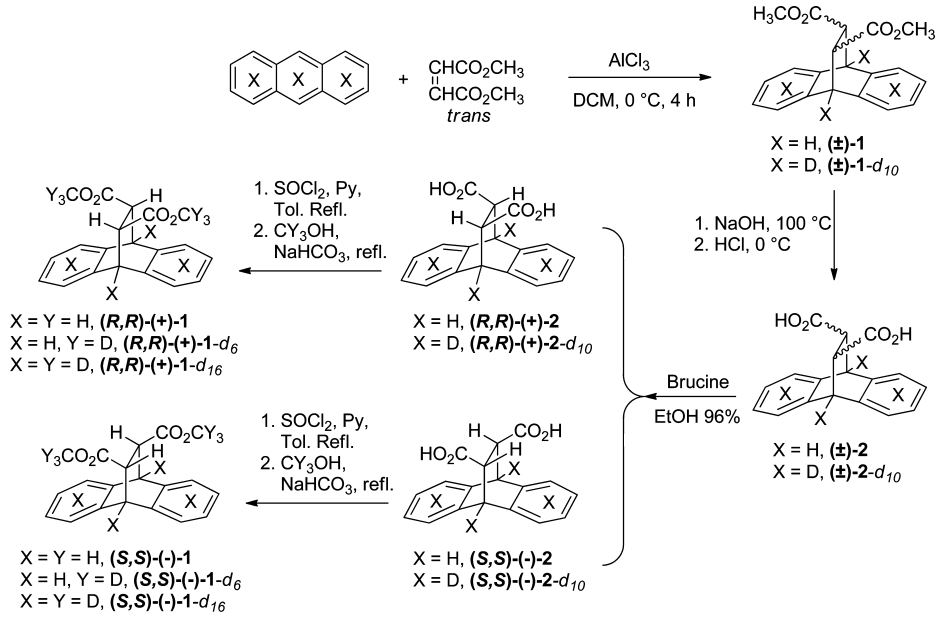

absorption (VA) and circular dichroism (VCD) spectra (as found in refs 17−20). Indeed, as it will be shown, this simplification of the spectra will allow us to gain significant insight regarding:

(1) the origin of the bands that dominate the VA and VCD peaks in the fingerprint region,
(2) the VCD bands in the CH-stretching region, which in this case presents unusually broad monosignate bands (we note these modes have been discussed for some time in the literature as typical of alcohols, acids, and esters and have been first rationalized in terms of the so-called ring-current mechanism[21−25])
(3) the bandshapes and bandwidths[26,27] of the VA and VCD spectra (these two important observables of VA and VCD spectra have been little investigated in the past, though it is clear that their understanding may help shed some light onto overall molecular motions in solution (e.g., translations, rotations, tumbling, etc.) as well as intramolecular relaxation phenomena (e.g., low-frequency/large-amplitude motions)).

In other words, the present study aims at investigating the fundamental chiroptical properties of this molecule and promises also to have the typical interesting applicative characteristics of adduct-type molecules, viz. the shape of the VA and VCD spectra of this type of compounds are influenced to a great extent by the large amplitude methoxy pseudorotation. With these goals in mind, systematic density functional theory (DFT) VA and VCD calculations have been performed for many structures of the considered molecules. That is to say, besides running calculations for the isolated molecule and molecular complexes formed between one solute molecule and two solvent molecules, the large amplitude methoxy pseudorotation has also been accounted for by performing linear transit calculations.

Of course we are confident that this basic study will also be appreciated outside fundamental science, because it is known that anthracene adducts are precursors of compounds widely used in different fields, such as medicinal chemistry,[28,29] stereoselective synthesis,[29,30] and material science.[31]

2. EXPERIMENTAL AND COMPUTATIONAL DETAILS

2.1. Synthesis and Characterization of adducts (*R,R*)-1, (*R,R*)-1-d_6, and (*R,R*)-1-d_{16} and Their Respective Enantiomers (*S,S*)-1, (*S,S*)-1-d_6, and (*S,S*)-1-d_{16}. The six stereoisomers have been synthesized ad hoc for this spectroscopic study and were derived from the common racemic dimethyl (±)-9,10-dihydro-9,10-ethanoanthracene-11,12-dicarboxylate, which has been prepared in very good yield (up to 90%) by $AlCl_3$-catalyzed Diels−Alder cycloaddition of dimethyl fumarate to both anthracene and its isotopomer anthracene-d_6 (Scheme 2).[32−36] s2

The alkaline hydrolysis of diester (±)-**1** and the deuterated analogue (±)-**1**-d_{10} provided the corresponding racemic acid (±)-**2** and (±)-**2**-d_{10}, which were resolved into the corresponding enantiomeric acids (*R,R*)-**2**, (*S,S*)-**2** and (*R,R*)-**2**-d_{10}, (*S,S*)-**2**-d_{10}, by fractional crystallization of their diastereomeric brucine salts. Each of the optically active acids was treated with thionyl chloride to obtain the corresponding acyl chlorides which was, finally, transformed into the esters (*R,R*)-**1**, (*S,S*)-**1**, and (*R,R*)-**1**-d_6, (*S,S*)-**1**-d_6 by refluxing of the acyl chlorides in methanol and methanol-d_4. (*R,R*)-**1**-d_{16}, and (*S,S*)-**1**-d_{16} were obtained analogously by refluxing the acyl chlorides of (*R,R*)-**2**-d_{10} and (*S,S*)-**2**-d_{10} in methanol-d_4.

See section SI-1, part (a) in the Supporting Information material for description of preparation and characterization of synthesized molecules and deuterated products. The products were fully characterized by elemental analysis, NMR, optical rotations measured in solutions at 24 °C, at the sodium D-line wavelength (589 nm) (OR), and electronic circular dichroism (ECD). The ECD spectra of the three isotopomers are reported in the Supporting Information in section SI-1, part (b), whereas the OR values and melting points (mp) are given in Table 1. t1

2.2. Infrared Absorption (VA) and Vibrational and Electronic Circular Dichroism (VCD and ECD) Spectra. IR

dx.doi.org/10.1021/jp502544v | J. Phys. Chem. A XXXX, XXX, XXX−XXX

Table 1. Experimental Melting Points and Specific Rotations at the Sodium D Line for Dimethyl (+)-(11*R*,12*R*)-9,10-Dihydro-9,10-ethanoanthracene-11,12-dicarboxylate ((*R*,*R*)-1**) and Dimethyl (−)-(11*S*,12*S*)-9,10-Dihydro-9,10-ethanoanthracene-11,12-dicarboxylate ((*S*,*S*)-**1**) and Two Isotopomers Thereof**

molecule	mp (°C)	$[\alpha]_D^{24}$ (*c*, 1.5, $CHCl_3$)	$[\alpha]_D^{24}$ (*c*, 1.5, CH_3OH)
(*R*,*R*)-**1**	89−91	+23.0	+21.1
(*S*,*S*)-**1**	90	−30.8	−21.3
(*R*,*R*)-**1**-d_6	88−90		+7.0
(*S*,*S*)-1-d_6	87−90		−7.8
(*R*,*R*)-**1**-d_{16}	91−92		+18.0
(*S*,*S*)-**1**-d_{16}	88−89		−20.0

absorption and VCD spectra were taken with a JASCO FVS4000 apparatus, equipped with two detectors, an MCT one employed in the mid-IR region from 900 to 1800 cm^{-1} and an InSb one employed in the CH-stretching region. In the two regions the same ZnSe photoelastic modulator (PEM) was used. Two transparent solvents for both spectral ranges were used, namely $CDCl_3$ and CD_3CN: no essential differences were noticed, notwithstanding the different polarity of the solvents. In the fingerprint region 2000 scans were taken and a 100 μm path length cell was employed, whereas for the CH-stretching region 5000 scans were taken and still a 100 μm cell was used. In either case the VA and VCD spectra for the solvent taken in the same conditions were subtracted. In the main text we provide the VCD spectra for the (*R*,*R*)-**1** enantiomers, obtained as semidifferences of the original VCD spectra of the (*R*,*R*)-**1** and (*S*,*S*)-**1** enantiomers (good mirror image spectra had been obtained).

ECD spectra (presented in section SI-1 of the Supporting Information, part (b)) were measured in 0.05 M/CH_3CN solutions contained in 0.1 mm quartz cuvettes, with 1 scan at 100 nm/min scanning speed using a Jasco815SE apparatus.

2.3. Computational Details. All calculations have been performed with the ADF program[37−40] package using the BP86 functional[41,42] and the ADF TZP[43] basis set. Both vacuum and COSMO[44−46] calculations have been performed. In the vacuum calculations all geometry optimizations and VA and VCD calculations have been performed for the isolated free molecules and molecular complexes. In the COSMO calculations the considered free molecules and molecular complexes were embedded in a dielectric continuum corresponding to chloroform (dielectric constant of 4.8). For brevity, we consider here only the results of the vacuum calculations for the molecular complexes formed between solute and solvent molecules, i.e., the calculations that have reproduced the experimental spectra best. (See section 4 in the Supporting Information (SI-4) for a comparison of all vacuum and COSMO VA and VCD spectra.)

The linear transit (LT) calculations, devised to simulate the pseudorotations of the methoxy groups, are performed in two steps. First, a set of intermediate structures (hereafter referred to as LT structures) is generated by varying a geometrical parameter (e.g., bond length, bond angle, dihedral angle) from an initial value to a final value in a given number of steps. The geometrical parameter (hereafter referred to as the LT parameter), its final value, and the number of LT steps are defined by the user in the beginning of the LT calculation. Then, a constrained geometry optimization is performed for each LT structure generated in the first step; i.e., the value of the LT parameter characterizing a given LT structure is kept fixed during the geometry optimization of all other structural parameters. (To obtain the reference structures, i.e., the structure used as the starting point for all LT calculations, stringent convergence criteria for the geometry optimizations where used, i.e., 1×10^{-4} hartree/Å for gradients. The convergence criteria used for the constrained geometry optimizations performed during the LT structure is 10^{-3} Hartree/Angstrom for gradients, i.e., ADF default.)

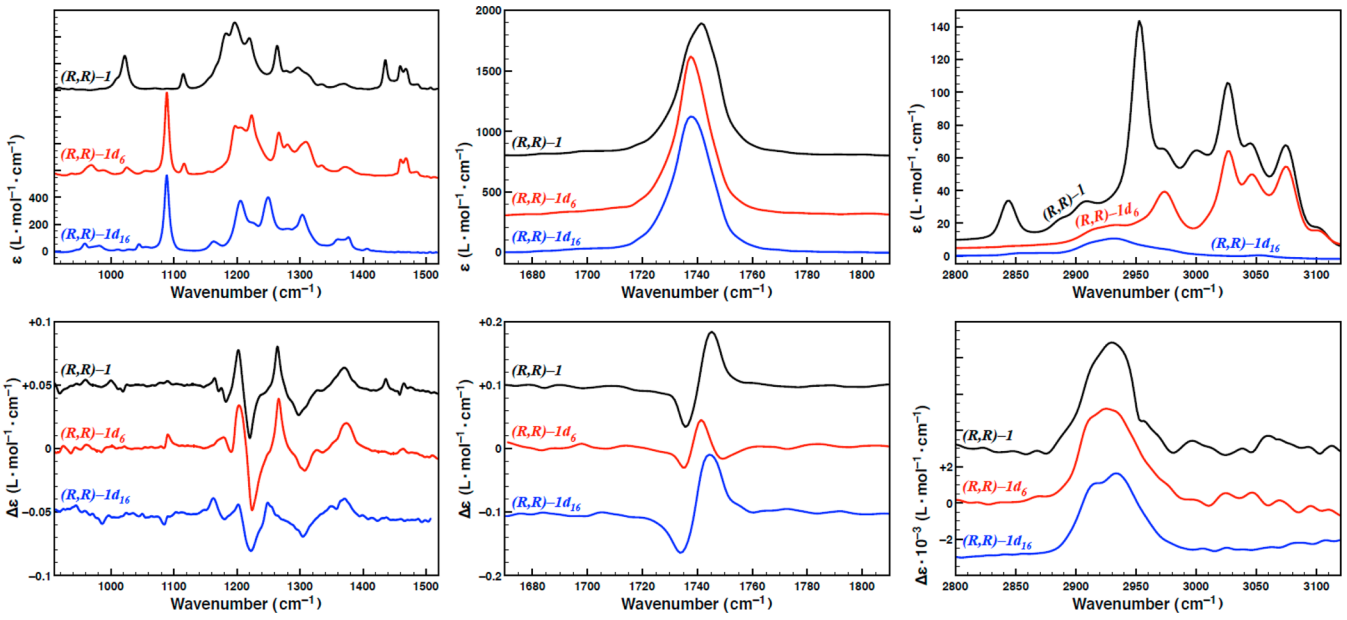

Figure 1. Comparison of experimental VA (upper panel) and VCD (lower panel) spectra of dimethyl-(+)-(11*R*,12*R*)-9,10-dihydro-9,10-ethanoanthracene-11,12-dicarboxylate and two deuterated isotopomers thereof, namely (*R*,*R*)-**1**, (*R*,*R*)-**1**-d_6, and (*R*,*R*)-**1**-d_{16} (Scheme 1) in the three spectroscopic regions: mid-IR (left), C═O stretching (center), and CH stretching (right). For experimental details see section 2.2.

dx.doi.org/10.1021/jp502544v | J. Phys. Chem. A XXXX, XXX, XXX−XXX

The simulated VA and VCD spectra were obtained by Lorentzian broadening of the dipole and rotational strength using a half-width of 8 cm^{-1}. The calculated harmonic frequencies have been scaled with the following factors: 1.02 in the fingerprint region and 0.985 in the C−H stretching. These values were found to provide the best agreement with observed VA and VCD band positions.

3. RESULTS AND DISCUSSION

3.1. Analysis of the Experimental VA and VCD Spectra. In Figure 1 we compare the experimental VA and VCD spectra of (*R*,*R*)-**1** and of its (*R*,*R*)-**1**-d_6 and (*R*,*R*)-**1**-d_{16} isotopomers, with the aim of identifying spectroscopic regions which are either constant or variable with deuteration.

In the first frequency region between 1000 and 1100 cm^{-1} the VA spectra of (*R*,*R*)-**1**-d_6 and (*R*,*R*)-**1**-d_{16} contain an intense band at 1090 cm^{-1} that is assigned to C−D bending modes of B symmetry (i.e., mostly umbrella motions localized on the two methoxy groups), coupled to C−O stretching modes. In (*R*,*R*)-**1** this band is not present at 1090 cm^{-1}, but another broad band is found at ca. 1040 cm^{-1} and further changes are noticed at higher frequencies (see below): this is due to CH_3 groups replacing CD_3 ones. The corresponding VCD signals are very weak.

In the next frequency region, i.e., between 1100 and 1400 cm^{-1}, the three VCD spectra exhibit fairly similar patterns. This suggests that the shape of the VCD spectra in this region is determined almost entirely by normal modes involving the two C*−H bonds (C* being either of the two stereogenic carbon atoms); possible contributions from CO and CC stretchings cannot be excluded, but their role is major in other spectroscopic regions. The three VA spectra, on the other hand, exhibit rather distinct features in this frequency interval, which indicates the VA spectra are more sensitive to movements of the C−H and C−D bonds than the VCD spectra.

Moving further to the C═O stretching region, i.e., to the 1650−1850 cm^{-1} frequency interval, one notices that the three molecules have fairly similar VA and VCD spectra. As shown in the middle panel of Figure 1, we have a broad IR band at ca. 1735 cm^{-1} and a (−, +) VCD couplet with the two components located at 1735 and at 1750 cm^{-1}, respectively. Given the fact that the carbonyl stretching modes are almost entirely localized on the C═O bonds (i.e., they are very little, if at all, contaminated by C−H bending modes), the similar appearances of the VA and VCD spectra of the three molecules are not surprising.

Finally, in the CH-stretching region, i.e., between 2800 and 3100 cm^{-1}, the quite structured VA spectrum of the (*R*,*R*)-**1** compound, containing all aromatic and aliphatic C−H stretching features, is reduced in the (*R*,*R*)-**1**-d_{16} isotopomer to a single broad band centered at 2920 cm^{-1}, which is determined solely by the stretching of the C*−H bonds. (Note that the spectrum of the (*R*,*R*)-**1**-d_6 isotopomer exhibits above 3000 cm^{-1} features associated only with the aromatic C−H stretching modes). As can be seen in the right panel of Figure 1, in correspondence with the broad VA band at 2920 cm^{-1}, a single broad positive band is observed in all three VCD spectra. This band is associated with the C*−H stretching modes.

As stated in the Introduction, the VCD signals associated with these C*−H stretching modes have long been recognized[21−25] as the prevailing signals in the VCD spectra of alcohols, acids, and esters. However, as the empirical analysis of VA and VCD spectra conducted above has shown, the VCD signals associated with normal modes involving the C*−H bonds dominate, not only in the C−H stretching region (2800 to 3200 cm^{-1}) but also in the fingerprint region between 1000 and 1400 cm^{-1} of the VCD spectra.

Finally, the many similarities and few characteristic differences observed in the VCD spectra of the tree isotopomers justify the decision to carry on the calculations just for the (*R*,*R*)-**1**-d_{16} molecule, because the interpretation of the VCD spectra of (*R*,*R*)-**1**-d_{16} will enable one to understand also the VCD spectra of (*R*,*R*)-**1**-d_6 and of (*R*,*R*)-**1** as well. The interpretation of VA spectra will come out as a consequence, too.

3.2. Standard DFT Calculations. *3.2.1. Molecular Structures.* The concluding remarks of section 3.1 led us to concentrate on calculations of geometries and spectra of (*R*,*R*)-**1**-d_{16}: of course we have also made sure that our predictions are equally good for the undeuterated or less deuterated species. (For ease of discussion we report in Scheme 3 the atom numbering of (*R*,*R*)-**1**-d_{16}, according to IUPAC convention.)

Scheme 3. Structure of Dimethyl (+)-(11*R*,12*R*)-9,10-Dihydro-9,10-ethanoanthracene-11,12-dicarboxylate, (*R*,*R*)-1, and Atom Numbering According to IUPAC, Used Throughout This Work

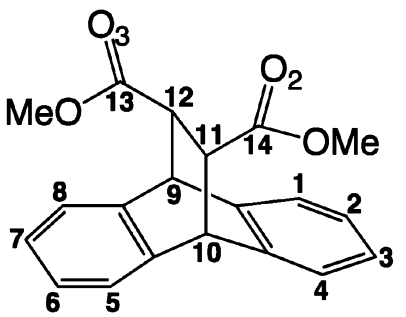

The conformers of (*R*,*R*)-**1**-d_{16} are determined by the relative orientations of its two C═O bonds. As indicated in Figure 2 by the orange arrows, there are three possibilities. That is to say, we have two conformers with C_2 symmetry (i.e., C^1 and C^2), and one conformer without symmetry (i.e., C^3). However,

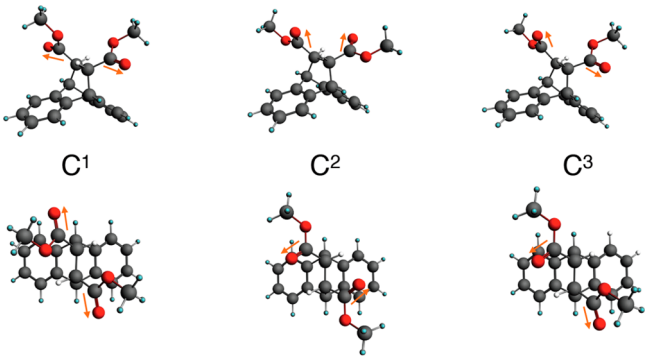

Figure 2. Optimized structures of the conformers C^1, C^2, and C^3 of dimethyl-(+)-(11*R*,12*R*)-9,10-dihydro-9,10-ethanoanthracene-11,12-dicarboxylate. Upper panel: viewed from a direction perpendicular to the C_2 symmetry axis (in conformers C^1 and/or C^2). Lower panel: viewed along the C_2 symmetry axis (in conformers C^1 and/or C^2). (The orange arrows indicate the direction of the C═O bonds.)

dx.doi.org/10.1021/jp502544v | J. Phys. Chem. A XXXX, XXX, XXX−XXX

because the conformer C^3 can be obtained in two ways (see section 2 in the Supporting Information), it must be counted twice, when VA and VCD spectra are calculated.

Further, because the two C=O bonds of (*R*,*R*)-**1**-d_{16} form intermolecular "hydrogen bonds" with deuterated chloroform solvent molecules (as noticed, e.g., in ref 47), we have performed calculations also for molecular complexes formed between one solute molecule and two solvent molecules, i.e., deuterated chloroform ($CDCl_3$). Three molecular complexes (MC) have been considered in total, i.e., one for each conformer. They are labeled as C^1-$(CDCl_3)_2$, C^2-$(CDCl_3)_2$, and C^3-$(CDCl_3)_2$.

Other relative geometries between $CDCl_3$ and (*R*,*R*)-**1**-d_{16} do not bear such low energies; two $CDCl_3$ molecules per (*R*,*R*)-**1**-d_{16} were considered on the basis of symmetry. The relative energies and the associated Boltzmann factors computed for the isolated conformers and also for the three molecular complexes are listed in Table 2. As can be seen, both sets of calculations predict the conformer C^2 and C^3 to be significantly populated at room temperature. That is, the Boltzmann factors computed for the two conformers are 0.60 (C^2) vs 0.36 (C^3) when the free molecules are considered, and 0.63 (C^2) vs 0.34 (C^3) when the molecular complexes with $CDCl_3$ solvent molecules are considered. (We note that similar results are obtained also with using the COSMO solvation model.)

Table 2. Relative Energies (Δ*E*) and Boltzmann Weights (BW) Computed for the Free Molecules (FM) and for the Molecular Complexes (MC (Computational Details: Vacuum, BP86, TZP)

conf.	Δ*E* (kcal/mol)	BW
	Free Molecule	
C^2	0.000	0.60
C^3_A	0.700	0.18
C^3_B	0.700	0.18
C^1	1.720	0.04
	Molecular Complex	
C^2-$(DCCl_3)_2$	0.000	0.63
C^3_B-$(DCCl_3)_2$	0.790	0.17
C^3_B-$(DCCl_3)_2$	0.790	0.17
C^1-$(DCCl_3)_2$	1.640	0.03

The optimized structures (BP86/TZP, vacuum) of the molecular complexes formed with the dominant conformers, i.e., C^2-$(CDCl_3)_2$ and C^3-$(CDCl_3)_2$, are shown in Figure 3.

3.2.2. Comparison of Experimental and Computed Spectra. Figure 4 shows comparisons between the experimental VA and VCD spectra of (*R*,*R*)-**1**-d_{16} and the spectra computed for the C^1-$(CDCl_3)_2$, C^2-$(CDCl_3)_2$, and C^3-$(CDCl_3)_2$ molecular complexes for the fingerprint region (comparisons of experimental and computed spectra of (*R*,*R*)-**1** and (*R*,*R*)-**1**-d_6 are shown in Section 5 of the Supporting Information) .

As can be seen in Figure 4, overall the spectra computed for the C^2-$(CDCl_3)_2$ complex reproduce the experimental spectra very well, and, at the same time, significantly better than the spectra computed for the other two conformers. On one hand, this is in agreement with the Boltzmann factors computed in Table 2 (which indicate that conformer C^2 is the predominant conformer). On the other hand, however, the spectra comparisons in Figure 4 suggest that even though the C^3-$(CDCl_3)_2$ conformer has been predicted to possess a significant population, very few signatures from the C^3-$(CDCl_3)_2$ conformer exist in the mid-IR VA and VCD spectra.

The analysis of the normal modes of conformer C^2 has shown that vibrational transitions associated with intense VA and VCD signals in the frequency interval between 1100 and 1400 cm^{-1} do indeed contain large contributions from C*−H bending modes. That is, 80% (or more) of the normal mode movements in these modes are localized on the C*−H bending

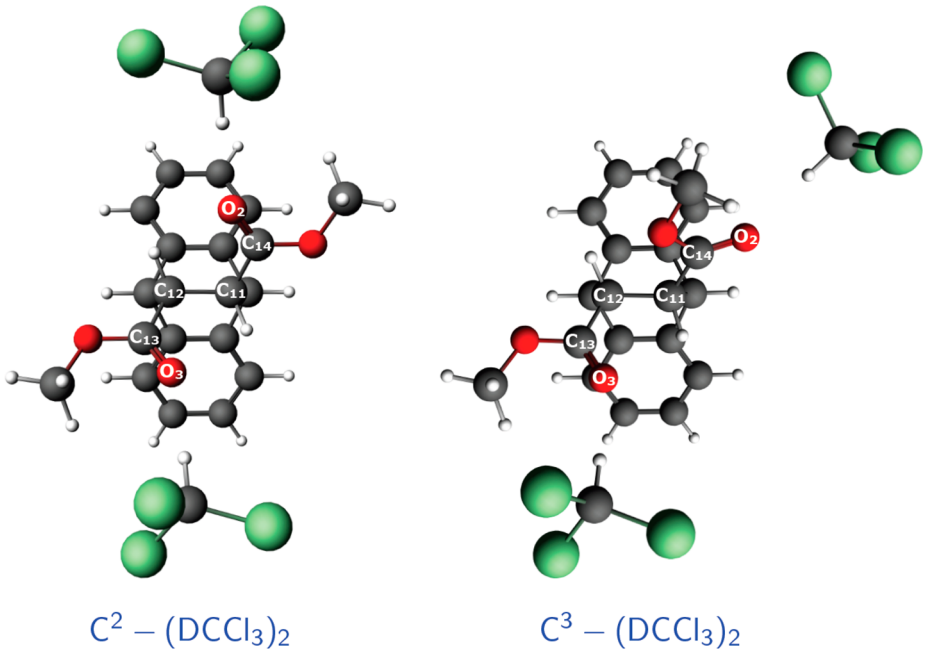

Figure 3. Optimized structures (BP86/TZP, vacuum) of the molecular complexes formed between the conformers C^3 (top panel) and C^2 (lower panel) of dimethyl-(+)-(11*R*,12*R*)-9,10-dihydro-9,10-ethanoanthracene-11,12-dicarboxylate-d_{16}, ((*R*,*R*)-**1**-d_{16}), and two $CDCl_3$ molecules, i.e., C^3-$(CDCl_3)_2$ and C^2-$(CDCl_3)_2$. (The atoms defining the dihedral angles varied during the linear transit (LT) calculations, i.e., $O_3C_{13}C_{12}C_{11}$ and $O_2C_{14}C_{11}C_{12}$ are highlighted in green.)

dx.doi.org/10.1021/jp502544v | J. Phys. Chem. A XXXX, XXX, XXX−XXX

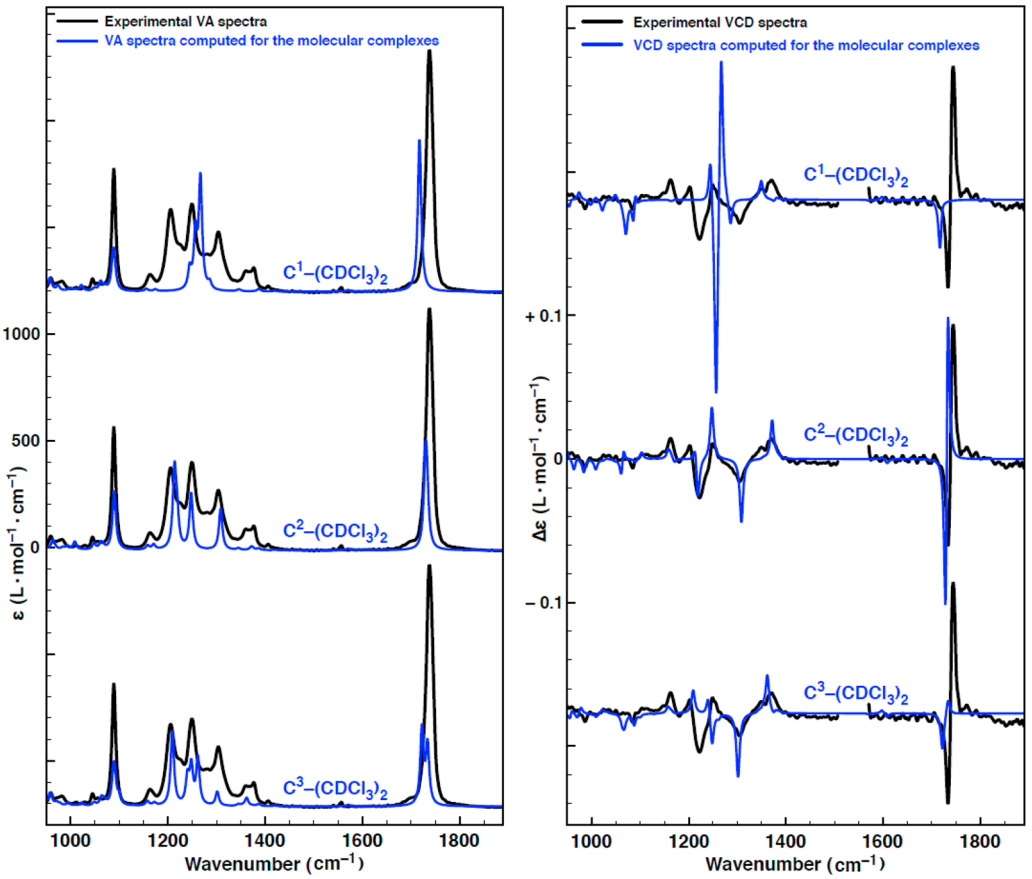

Figure 4. Fingerprint spectral region: comparison of the experimental VA (left) and VCD (right) spectra of dimethyl-(+)-(11*R*,12*R*)-9,10-dihydro-9,10-ethanoanthracene-11,12-dicarboxylate-d_{16}, (*R*,*R*)-**1**-d_{16}, measured in $CDCl_3$ to spectra calculated for the C^1-$(CDCl_3)_2$, C^1-$(CDCl_3)_2$, and C^3-$(CDCl_3)_2$ molecular complexes. Computational details: BP86/TZP, vacuum, isolated conformers.

modes (with the remaining 20% consisting of C−C and/or C−O stretching modes). This confirms the conclusions drawn in section 3.1; i.e., not only the CH stretching region of the spectra but also the fingerprint region between 1100 and 1400 cm^{-1} is determined by the modes localized on the C*−H bonds.

In the carbonyl stretching region, i.e., between 1700 and 1800 cm^{-1}, the VA spectra present a strong and broad band, whereas the VCD spectra exhibit a couplet with (−, +) signs in order of increasing wavenumbers. This feature is very well reproduced by the spectrum computed for the C^2-$(CDCl_3)_2$ complex—we have a very intense bisignate doublet (determined by C═O stretching modes) with a negative band, at 1730 cm^{-1} (B symmetry) and a positive one at 1733 cm^{-1} (A symmetry).

We note that the performed normal-mode analysis confirms that the observed signs ~~are~~ can be explained by the vibrational coupled dipoles mechanism, discussed in the early days of VCD by Holzwarth,[48] later studied by ab initio methods by Bouř and Keiderling,[49] and recently thoroughly discussed, on the basis of DFT calculations, by Taniguchi and Monde.[50] In accordance with the exciton chirality rule formulated by Taniguchi and Monde,[50] in the (*R*,*R*)-**1** case one C═O bond has to be rotated anticlockwise to eclipse the other C═O bond, providing the (−) case, as observed in all experimental and calculated VCD spectra in Figures 1 and 4.

It is also interesting to note that in the fingerprint region, the agreement between experimental and computed spectra seems to be better for the VCD spectra than for the VA spectra (not only for the C^2-$(CDCl_3)_2$ spectra but also for the Boltzmann averages shown later in Figure 8). The relative intensities of the various bands in the fingerprint region are predicted in the simulated VCD spectra better than in the VA ones, where the carbonyl stretching bands should be significantly more intense than the rest of the bands.

In the CH-stretching region, both VA and VCD experimental spectra are quite simple and consist of a single positive feature, which in both cases is quite broad though not very intense. As can be seen in Figure 5, all computed spectra provide a good description of experimental ones; viz., in all cases the predicted bands have the correct VCD sign and have good enough VA and VCD intensities (the same can be said about the prediction of VA and VCD spectra in the CH-stretching region for (*R*,*R*)-**1**, Figure SI-5, Supporting Information). However, in spite of their simplicity, the spectra in CH-stretching region, unlike the rich fingerprint spectra, seem to provide evidence that, as predicted in Table 2, conformer C^3 is also populated in the experimental sample. Indeed, in both VA and VCD spectra, the single peak calculated for the C^2-$(CDCl_3)_2$ spectra is positioned in correspondence with the most intense experimental band. At the same time, this peak is situated right between the two peaks obtained in the C^3-$(CDCl_3)_2$ spectra whose positions also agree quite well with the positions of the shoulders observed in the experimental spectra. Regarding the assignment of the bands in the 2800−3000 cm^{-1} frequency interval, as discussed in section 3.1, all peaks in the computed spectra are associated to C*−H stretching modes. We note that, although the importance of this VCD band in numerous cases encompassing alcohols,

dx.doi.org/10.1021/jp502544v | J. Phys. Chem. A XXXX, XXX, XXX−XXX

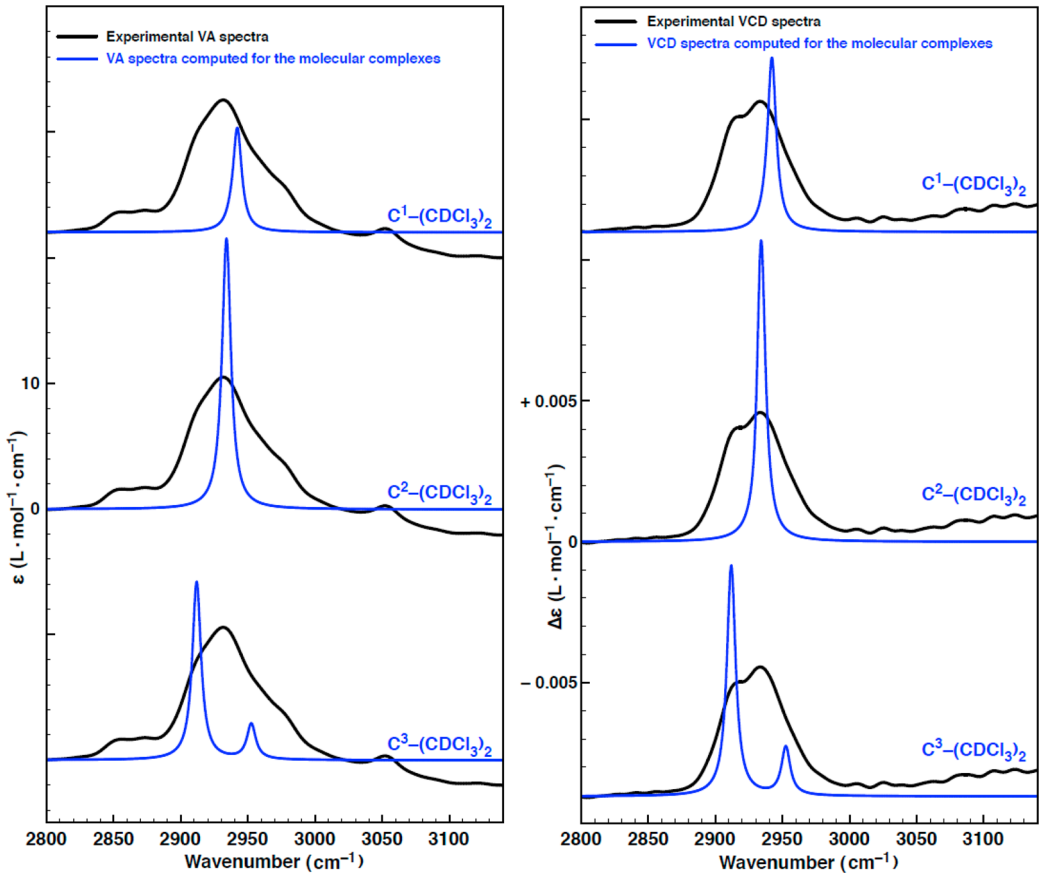

Figure 5. CH stretching regions: comparison of the experimental VA (left) and VCD (right) spectra of dimethyl-(+)-(11*R*,12*R*)-9,10-dihydro-9,10-ethanoanthracene-11,12-dicarboxylate-d_{16}, (*R*,*R*)-**1**-d_{16}, measured in $CDCl_3$ to spectra calculated for the C^1-$(CDCl_3)_2$, C^1-$(CDCl_3)_2$, and C^3-$(CDCl_3)_2$ molecular complexes. Computational details: BP86/TZP, vacuum, isolated conformers.

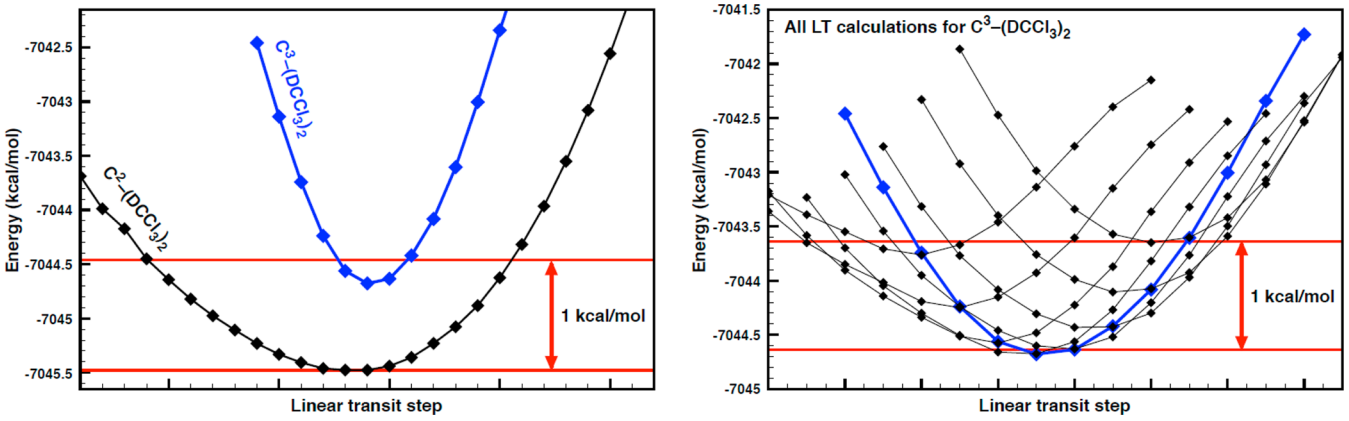

Figure 6. Variation of the energy of dimethyl-(+)-(11*R*,12*R*)-9,10-dihydro-9,10-ethanoanthracene-11,12-dicarboxylate-d_{16}, (*R*,*R*)-**1**-d_{16}, during the LT scans. Left panel: (1) Energy dependence of C^2-$(CDCl_3)_2$ on the dihedral angles $O_3C_{13}C_{12}C_{11}$ and $O_2C_{14}C_{11}C_{12}$ (black curve). The two angles were varied symmetrically in steps of ±3° to preserve the C_2 symmetry of C^2-$(CDCl_3)_2$. (2) Energy dependence of C^3-$(CDCl_3)_2$ on the dihedral angles $O_3C_{13}C_{12}C_{11}$ (blue curve). The angle was varied in steps of ±10° whereas the second dihedral angle, i.e., $O_2C_{14}C_{11}C_{12}$, angle was not varied as C^3-$(CDCl_3)_2$ does not have symmetry. Right panel: (1) Energy dependence of C^3-$(CDCl_3)_2$ on the $O_2C_{14}C_{11}C_{12}$ dihedral angle (black curve). The $O_2C_{14}C_{11}C_{12}$ LT scans have been performed for each $O_3C_{13}C_{12}C_{11}$ value (i.e., diamond on the blue curve) situated in the highlighted 1 kcal/mol interval. $O_2C_{14}C_{11}C_{12}$ was varied in steps of ±10°. (2) (Blue) C^3-$(CDCl_3)_2$ energy curve in the left panel which shows the $O_3C_{13}C_{12}C_{11}$ values for which $O_2C_{14}C_{11}C_{12}$ LT scans have been performed. (See Figure 3 and Scheme 3 for definition of dihedral angles involved in LT calculations.)

sugars, acids, amino acids, and esters has been recognized by Nafie et al.[21−23] already in 1986, the mechanism responsible for this rather intense VCD band is still a matter of discussion.[24,25]

We can therefore conclude that the standard DFT calculations performed for the C^1-$(CDCl_3)_2$, C^2-$(CDCl_3)_2$, and C^3-$(CDCl_3)_2$ molecular complexes have yielded spectra that overall reproduce the experimental ones quite well (as shown in section 5 in the Supporting Information, this is the case for (*R*,*R*)-**1** and (*R*,*R*)-**1**-d_6). However, there are still a few details in the experimental spectra that are not well reproduced

dx.doi.org/10.1021/jp502544v | J. Phys. Chem. A XXXX, XXX, XXX−XXX

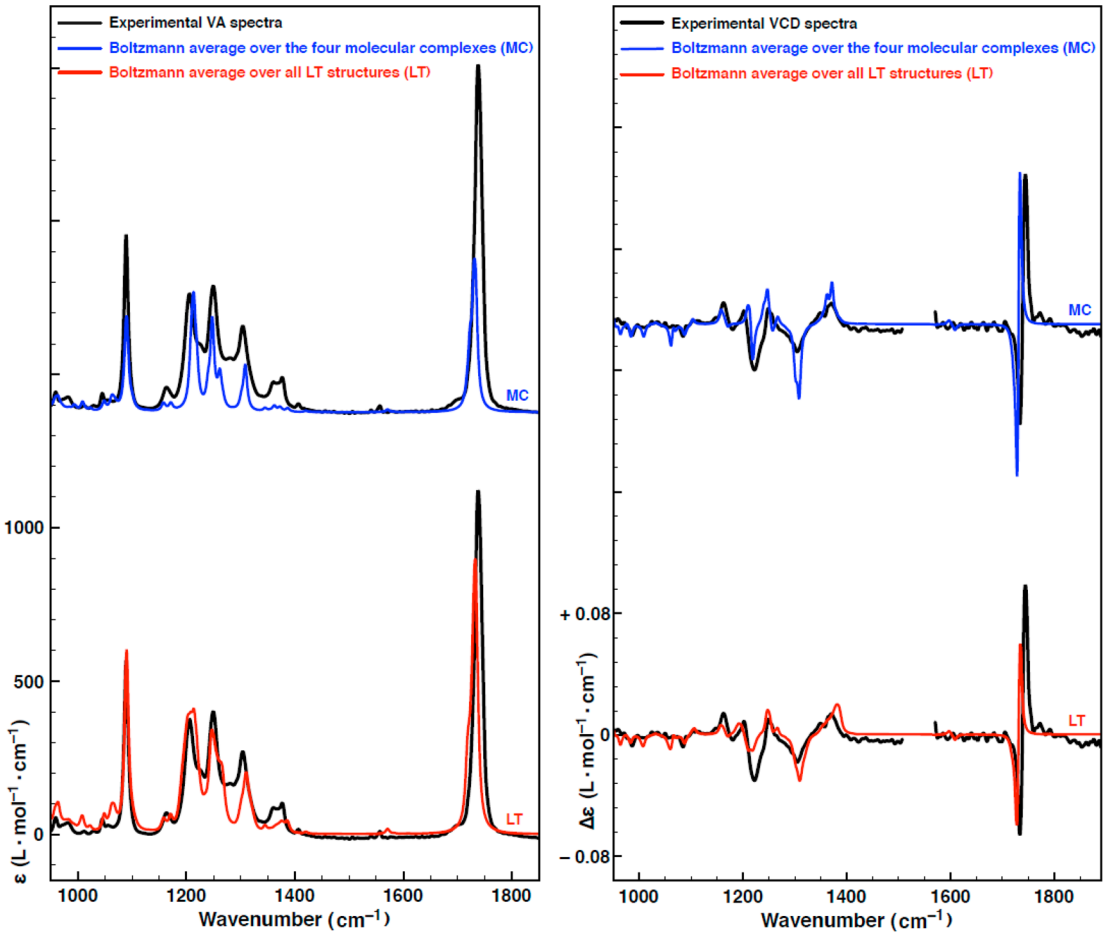

Figure 7. Fingerprint spectral region: comparison of experimental and Boltzmann weighted VA (left) and VCD (right) spectra of dimethyl-(+)-(11*R*,12*R*)-9,10-dihydro-9,10-ethanoanthracene-11,12-dicarboxylate-d_{16}, (*R*,*R*)-**1**-d_{16}. The upper spectra (in blue), labeled MC, are Boltzmann averages over the spectra computed for the "steady" molecular complexes formed with the three conformers (the Boltzmann factors are given in Tables 2). The lower spectra (in red), labeled LT, are Boltzmann averages over all spectra computed for the (*R*,*R*)-**1**-d_{16} molecule, i.e., the spectrum computed for C^1-$(CDCl_3)_2$, and the spectra computed for the C^2-$(CDCl_3)_2$ and C^3-$(CDCl_3)_2$ LT structures.

by these calculations, namely, (1) the relative intensities bands (most notably in the in the fingerprint VA spectra) and (2) the broad character of some experimental bands. Both these issues will be discussed in the next section.

3.2.3. Linear Transit Calculations. To simulate the effects induced in the spectra by the large amplitude pseudorotations performed by the two methoxy groups, the relative orientation of the two carbonyl groups was systematically varied by performing linear transit (LT) calculations (described in section 2.3) for the C^2-$(CDCl_3)_2$ and C^3-$(CDCl_3)_2$ molecular complexes. This approach had been tried somewhat empirically previously,[51−55] but here we propose to Boltzmann average the VA and VCD spectra of all LT structures, as for hindered rotations or torsions defining flat energy curves, it is practically impossible to define an absolute energy minimum. Two dihedral angles have been varied during the LT calculations, i.e., $O_3C_{13}C_{12}C_{11}$ and $O_2C_{14}C_{11}C_{12}$ (the atoms defining these two angles are shown in Figure 3; see also the IUPAC numbering in Scheme 3). In the case of the C^2-$(CDCl_3)_2$ molecular complexes, which has C_2 symmetry, the two dihedral angles have been varied symmetrically (i.e., to preserve the C_2 symmetry) by ±48° in steps of 3° starting from their initial value of 6°. In the case of the C^3-$(CDCl_3)_2$ complexes, which does not belong to the C_2-symmetry group, we have first run a LT calculation for the $O_3C_{13}C_{12}C_{11}$ angle (see the blue energy curve in the left panel in Figure 6), then for each LT structures whose energy was within 1 kcal/mol with respect to the reference C^3-$(CDCl_3)_2$ structure, we have run additional LT calculations for the $O_2C_{14}C_{11}C_{12}$ angle (see the right panel in Figure 6). In this case, the two angles have been varied by ± 60° in steps of 10°, viz. to sample significantly different spectra, a larger LT step was needed in the case of C^3-$(CDCl_3)_2$. The variation of the energy during these linear transit scans is shown in Figure 6.

VA and VCD calculations have been performed for all LT structures within the 1 kcal/mol energy intervals highlighted in the left and right panels of Figure 6, i.e., for 17 C^2-$(CDCl_3)_2$ LT structures and for 48 C^3-$(CDCl_3)_2$ LT structures.

Finally, we note that the high frequency modes in the fingerprint and CH stretching regions (in which we are interested) are associated with coordinates that have been fully optimized during the LT scans; i.e., they do not involve the coordinates defining the pseudorotations of the two methoxy groups that have been only partially optimized during the LT scans. Consequently, these modes are predicted accurately by the frequency calculations performed here for the partially optimized LT structures.[56]

Figures 7 and 8 show comparisons between the experimental VA and VCD spectra and simulated spectra. The simulated spectra reported in the upper part of each plot in Figures 7 and

dx.doi.org/10.1021/jp502544v | J. Phys. Chem. A XXXX, XXX, XXX−XXX

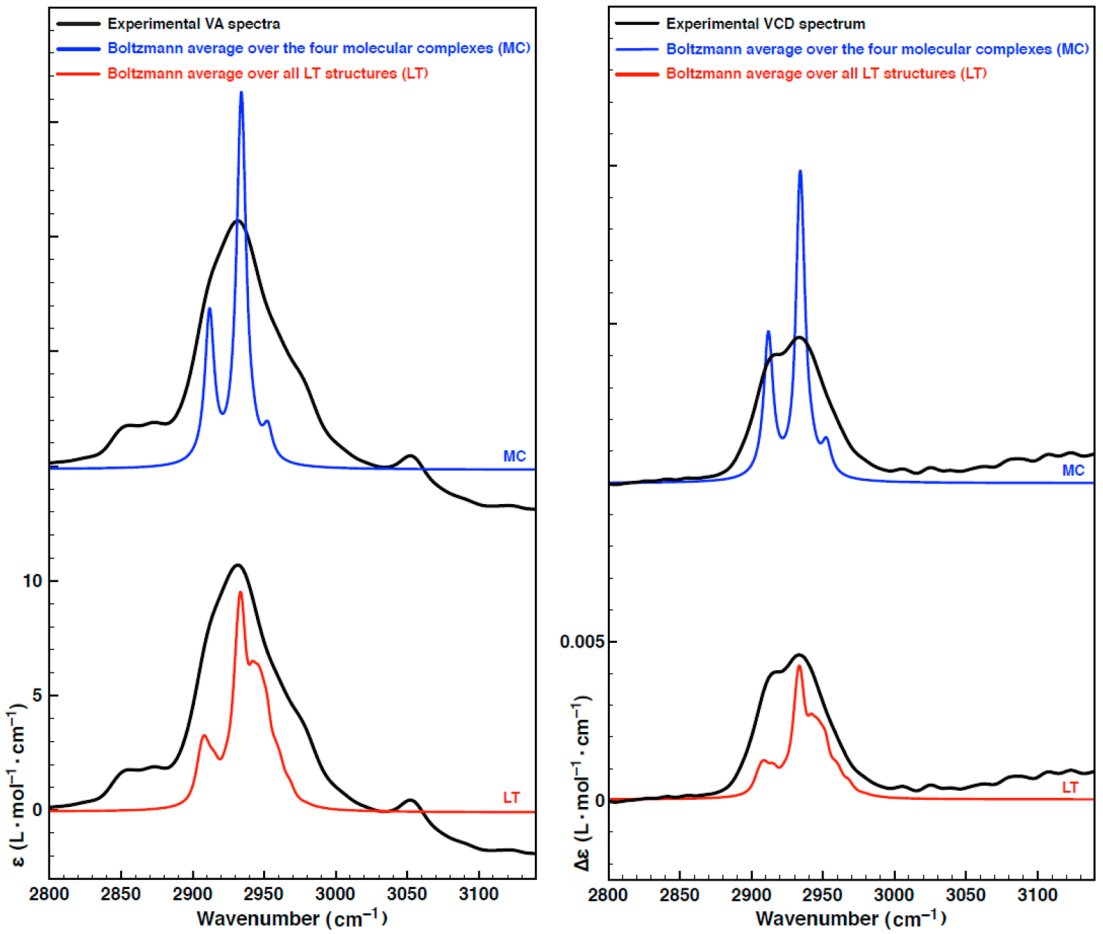

Figure 8. C−H stretching regions: comparison of experimental and Boltzmann weighted VA (left) and VCD (right) spectra of dimethyl-(+)-(11*R*,12*R*)-9,10-dihydro-9,10-ethanoanthracene-11,12-dicarboxylate-d_{16}, (*R*,*R*)-**1**-d_{16}. The upper spectra (in blue), labeled MC, are Boltzmann averages over the spectra computed for the "steady" molecular complexes formed with the three conformers (the Boltzmann factors are given in Tables 2). The lower spectra (in red), labeled LT, are Boltzmann averages over all spectra computed for the (*R*,*R*)-**1**-d_{16} molecule, i.e., the spectrum computed for C^1-$(CDCl_3)_2$, and the spectra computed for the C^2-$(CDCl_3)_2$ and C^3-$(CDCl_3)_2$ LT structures.

8 (labeled as MC) have been obtained as Boltzmann averages of the spectra computed for the fully optimized structures of the molecular complexes C^1-$(CDCl_3)_2$, C^2-$(CDCl_3)_2$, and C^3-$(CDCl_3)_2$. The simulated spectra in the lower part of Figures 7 and 8 (labeled as LT) have been obtained as Boltzmann averages over all spectra computed for the (R,R)-**1**-d_{16} molecule, i.e., the spectrum computed for C^1-$(CDCl_3)_2$, and all spectra computed for the C^2-$(CDCl_3)_2$ and C^3-$(CDCl_3)_2$ LT structures. More specifically, to preserve the Boltzmann populations in Table 2, the C^2-$(CDCl_3)_2$ and C^3-$(CDCl_3)_2$ sets of LT spectra have been first averaged separately using the energies obtained during the LT scans, viz. we have much more LT structure for the conformer C^3-$(CDCl_3)_2$ than for conformer C^2-$(CDCl_3)_2$. Then, the two Boltzmann weighted spectra obtained for the C^2-$(CDCl_3)_2$ and C^3-$(CDCl_3)_2$ LT structures, have been averaged together with the spectrum computed for conformer C^1-$(CDCl_3)_2$ using the Boltzmann factors given in Table 2.

The spectra comparisons in Figures 7 will be discussed first. In the case of the VA spectra, the LT simulated spectrum reproduces the experimental spectrum significantly better than the MC simulated spectrum; viz., the LT spectrum reproduces the relative magnitude of the various bands in the experimental spectrum significantly better than the MC spectrum. The LT spectrum improves upon the MC spectrum also when at the VCD spectra are reviewed, notice in particular the bandwidths of the (−, +) doublet observed in experiment at ca. 1300 and 1370 cm^{-1}, which are calculated broader, whereas all other couplets are narrow and the same as in the MC case and as observed.

The C−H stretching region (see Figures 8), which is essentially due to local C*−H stretching modes in all conformers, is better evaluated by the LT approach, as far as the bandwidth and intensity is concerned, for both VA and VCD spectra. Although the MC spectra provide a very good representation of the experimental spectra with the narrow bands falling right on top of the peaks and shoulders observed in the experimental spectra, LT calculations appear to distribute the C*−H frequencies around the two main peaks for the C^2 and C^3 conformers over a wider region. Indeed, in this region a crucial role is played by the frequency of the C−H stretching modes in the two conformers. A long time ago[57] the dependence of C−H stretching frequency with respect to the lone pairs of a nearby oxygen atom was studied and subsequently proved by ab initio techniques.[58] Those findings as well as the present ones may have some relevance in the dispute of the ring-current mechanism, introduced to rationalize VCD spectra of a C*−H bond in alcohols, acids, etc.[21−25] Indeed, all previous observations about CH-stretching VCD spectra in alcohols, esters, amines, etc. have reported broad and

dx.doi.org/10.1021/jp502544v | J. Phys. Chem. A XXXX, XXX, XXX−XXX

intense C*−H features. Our explanation of the band shape is thought to corroborate the previous quoted evidence.

4. CONCLUSIONS

In this work we have presented a fundamental VA and VCD study using as example the dimethyl-(+)-(11*R*,12*R*)-9,10-dihydro-9,10-ethanoanthracene-11,12-dicarboxylate molecule and two deuterated isotopomers specially synthesized for this study with a chemical structure endowed with C_2 symmetry. The spectra are particularly "clean" and the VCD spectrum in the fingerprint region consists of doublets of alternating sign, whereas in the C−H stretching region it contains a single broad band. The simplicity of the spectra is traced back in the symmetry of the molecule and the extensive use of deuteration.

The comparisons of the VCD spectra measured for the undeuterated and the two deuterated species has demonstrated clearly that the normal modes involving movements of the C*−H bonds (C* being either of the two stereogenic carbon atoms) determine the shape of the VCD spectra not only in the C−H stretching region but also in the fingerprint region. Though C*−H stretchings were thoroughly investigated in the past,[21−25] the C*−H rockings and bendings modes have been considered only recently.[52]

The computed DFT spectra reproduce well the experiment and allowed to confirm the crucial role of played by the C*−H rocking, bending and stretching modes. Moreover, comparisons of the experimental and computed spectra have shown that more information about the conformer distribution from experimental data can be obtained by considering both the fingerprint and the CH stretching regions. Best computations are obtained by considering the effect of the solvent, through the introduction of explicit solvent molecule.

Finally, taking into account the large amplitude torsional motions of the methoxy moieties through the linear transit (LT) method allows one to improve the quality of both VA and VCD calculated spectra, as compared to experimental results, especially in regard to relative intensities and bandwidths. Indeed, not only were we able to predict a broad and structured C−H stretching VCD band, but we were also able to understand why only one VCD couplet in the mid-IR region is broad, whereas all others are narrow.

■ ASSOCIATED CONTENT

Supporting Information

SECTION SI-1 (a): Synthesis and characterization of adducts (*R*,*R*)-**1**, (*R*,*R*)-**1**-d_6, and (*R*,*R*)-**1**-d_{16} and their respective enantiomers (*S*,*S*)-**1**, (*S*,*S*)-**1**-d_6, and (*S*,*S*)-**1**-d_{16}. SECTION SI-1 (b): ECD and UV absorption spectra of (*R*,*R*)-**1** and (*S*,*S*)-**1**. SECTION SI-2: Conformers C^3_A and C^3_B. SECTION SI-3: Anthracene dihedral angle. SECTION SI-4: Vacuum, COSMO, and LT calculations for C^2- and C^3-$(CDCl_3)_2$ (TBE vs LT parameters, VA and VCD spectra). SECTION SI-5: Comparison of vacuum calculations for (*R*,*R*)-**1** and (*R*,*R*)-**1**-d_{16} in the C^2-conformation (VA and VCD spectra). This information is available free of charge via the Internet at http://pubs.acs.org

■ AUTHOR INFORMATION

Corresponding Author

*S. Abbate: e-mail, abbate@med.unibs.it.

Present Address

[⊥]Dipartimento di Chimica, Materiali e Ingegneria Chimica "G. Natta" − Politecnico di Milano, Piazza Leonardo da Vinci 32, 20133 Milano, Italy.

Notes

The authors declare no competing financial interest.

■ ACKNOWLEDGMENTS

This work was supported by The Netherlands' Foundation for Scientific Research (VENI grant VPN). S.A., G.L., and R.R. thank the Italian "Ministero dell'Istruzione, dell'Università e della Ricerca" (MIUR) for financial support, under the auspices of the program PRIN 2008LYSEBR. M.P. thanks the HPC program (EU) for the HPC-Europa2 transnational program fellowship that has allowed him to visit the lab of V.P.N. for two months.

■ REFERENCES

(1) Cahn, R-S.; Ingold, C. K.; Prelog, V. Specification of Molecular Chirality. *Angew. Chem., Int. Ed.* **1966**, *5*, 385−415.

(2) Mislow, K. *Introduction to Stereochemistry*; W. A. Benjamin, Inc.: New York, Amsterdam, 1965

(3) Berova, N.; Polavarapu, P. L.; Nakanishi, K.; Woody, R. W. *Comprehensive Chiroptical Spectroscopy*; John Wiley & Sons: New York, 2012; Vols. *1*−*2*.

(4) Stephens, P. J. Vibrational Circular Dichroism Spectroscopy: A New Tool for the Stereochemical Characterization of Chiral Molecules. In *Computational Medicinal Chemistry for Drug Discovery*; Bultinck, P., de Winter, H., Langenaecker, W., Tollenaere, J., Eds.; Dekker: New York, 2003; pp 699−725.

(5) Stephens, P. J.; Devlin, F. J.; Pan, J.J . The Determination of the Absolute Configurations of Chiral Molecules Using Vibrational Circular Dichroism (VCD) Spectroscopy. *Chirality* **2008**, *20*, 643−663.

(6) Nafie, L. A.; Freedman, T. B. Vibrational Optical Activity Theory. In: *Circular Dichroism: Principles and Applications*, 2nd ed.; Berova, N., Nakanishi, K., Woody, R. W., Eds.; Wiley-VCH: New York, 2000; pp 97−152.

(7) Nafie, L. A. *Vibrational Optical Activity, Principles and Applications*; John Wiley and Sons: New York, 2011

(8) Keiderling, T. A. Peptide and Protein Conformational Studies with Vibrational Circular Dichroism and Related Spectroscopies. In *Circular Dichroism: Principles and Applications*. Nakanishi, K., Berova, N., Woody, R. W., Eds.; Wiley-VCH: New York; 2000; pp 621−666.

(9) Polavarapu, P. L.; Zhao, C. Vibrational Circular Dichroism: A New Spectroscopic Tool for Biomolecular Structural Determination. *Fresenius J. Anal. Chem.* **2000**, *366*, 727−734.

(10) Nicu, V. P.; Neugebauer, J.; Baerends, E. J. Effects of Complex Formation on Vibrational Circular Dichroism Spectra. *J. Phys. Chem. A* **2008**, *112*, 6978−6991.

(11) Nicu, V. P.; Debie, E.; Herrebout, W.; Van Der Veken, B.; Bultink, P.; Baerends, E. J. A VCD Robust Mode Analysis of Induced Chirality: The Case of Pulegone in Chloroform. *Chirality* **2009**, *21*, E287−E297.

(12) Polavarapu, P. L.; Frelek, J.; Woznica, M . Determination of the Absolute Configurations Using Electronic and Vibrational Circular Dichroism Measurements and Quantum Chemical Calculations. *Tetrahedron: Asymmetry* **2011**, *22*, 1720−1724.

(13) Bouchet, A.; Brotin, T.; Linares, M.; Agren, H.; Cavagnat, D.; Buffeteau, T. Conformational Effects Induced by Guest Encapsulation in an Enantiopure Water-Soluble Cryptophane. *J. Org. Chem.* **2011**, *76*, 1372−1383.

(14) Stephens, P. J.; Devlin, F. J.; Gasparrini, F.; Ciogli, A.; Spinelli, D.; Cosimelli, B. Determination of the Absolute Configuration of a Chiral Oxadiazol-3-one Calcium Channel Blocker, Resolved Using Chiral Chromatography, via Concerted Density Functional Theory

Calculations of Its Vibrational Circular Dichroism, Electronic Circular Dichroism, and Optical Rotation. *J. Org. Chem.* **2007**, *72*, 4707−4715.
(15) Abbate, S.; Longhi, G.; Gangemi, R.; Giorgio, E.; Rosini, C. Fenchone, Camphor, 2-methylenefenchone, and 2-methylenecamphor: A Vibrational Circular Dichroism Study. *J. Phys. Chem. A* **2006**, *110*, 4958−4968.
(16) Abbate, S.; Burgi, L. F.; Gangemi, F.; Gangemi, R.; Lebon, F.; Longhi, G.; Pultz, V. M.; Lightner, D. A. Comparative Analysis of IR and Vibrational Circular Dichroism Spectra for a Series of Camphor-related Molecules. *J. Phys. Chem. A* **2009**, *113*, 11390−11405.
(17) Abbate, S.; Longhi, G.; Gangemi, F.; Gangemi, R.; Superchi, S.; Caporusso, A. M.; Ruzziconi, R. Electrical and Mechanical Anharmonicities from NIR-VCD Spectra of Compounds Exhibiting Axial and Planar Chirality: The Case of (*S*)-2,3-Pentadiene and Methyl-d_3-[2.2]paracyclophane-4-carboxylate. *Chirality* **2011**, *23*, 841−849.
(18) Freedman, T. B.; Spencer, K. M.; Ragunathan, N.; Nafie, L. A.; Moore, J. A.; Schwab, J. M. Vibrational Circular Dicshroism of (*S*,*S*)-[2,3-$^2H_2$]oxirane in the Gas Phase and in Solution. *Can. J. Chem.* **1991**, *69*, 1619−1629.
(19) Narayanan, U.; Keiderling, T. A.; Elsevier, C.; Vermeers, P.; Runge, W. Vibrational Circular Dichroism of Optically Active Substituted Allenes: Experimental Results. *J. Am. Chem. Soc.* **1988**, *110*, 4133−4138.
(20) Narayanan, U.; Keiderling, T. A. Vibrational Circular Dichroism of Optically Active Substituted Allenes: Calculational Results. *J. Am. Chem. Soc.* **1988**, *110*, 4139−4144.
(21) Nafie, L. A.; Freedman, T. B. Ring Current Mechanism of Vibrational Circular Dichroism. *J. Phys. Chem.* **1986**, *90*, 763−767.
(22) Paterlini, M. G.; Freedman, T. B.; Nafie, L-A. Ring Current Enhanced Vibrational Circular Dichroism in the CH-Stretching Motions of Sugars. *J. Am. Chem. Soc.* **1986**, *108*, 1389−1397.
(23) Gigante, D. M. P.; Long, F.; Bodack, L. A.; Evans, J. M.; Kallmerten, J.; Nafie, L. A.; Freedman, T. B. Hydrogen Stretching Vibrational Circular Dichroism in Methyl Lactate and Related Molecules. *J. Phys. Chem. A* **1999**, *103*, 1523−1537.
(24) Bursi, R.; Stephens, P. J. Ring Current Contributions to Vibrational Circular Dichroism? Ab Initio Calculations for Methyl Glycolate-*d*, and $-d_4$. *J. Phys. Chem.* **1991**, *95*, 6447−6454.
(25) Bursi, R.; Devlin, F. J.; Stephens, P. J. Vibrationally Induced Ring Currents? The Vibrational Circular Dichroism of Methyl Lactate. *J. Am. Chem. Soc.* **1990**, *112*, 9430−9432.
(26) Gordon, R. G. Molecular Motion in Infrared and Raman Spectra. *J. Chem. Phys.* **1965**, *43*, 1307−1312.
(27) Abbate, S.; Longhi, G.; Kwon, K.; Moscowitz, A. The Use of Cross-correlation Functions in the Analysis of Circular Dichroism Spectra. *J. Chem. Phys.* **1998**, *108*, 50−61.
(28) Alibert, S.; Santelli-Rouvier, C.; Castaing, M.; Berthelot, M.; Spengler, G.; Molnar, J.; Barbe, J. Effects of a Series of Dihydroanthracene Derivatives on Drug Efflux in Multidrug Resistant Cancer Cells. *Eur. J. Med. Chem.* **2003**, *38*, 253−263.
(29) Naidu, A. B.; Jaseer, E. A.; Sekar, G. General, Mild, and Intermolecular Ullmann-type Synthesis of Diaryl and Alkyl Aryl Ethers Catalyzed by Diol-copper(I) Complex. *J. Org. Chem.* **2009**, *74*, 3675−3679.
(30) Le Maux, P.; Dorcet, V.; Simonneau, G. Asymmetric Copper-catalyzed Diels-Alder Reaction Revisited: Control of the Structure of Bis(oxazoline) Ligands. *Tetrahedron* **2013**, *69*, 8291−8298.
(31) Rabjohns, M. A.; Hodge, P.; Lovell, P. A. Synthesis of Aromatic Polyamides Containing Anthracene Units Via a Precursor Polymer Approach. *Polymer* **1997**, *38*, 3395−3407.
(32) Brienne, M.-J.; Jacques, J. Etude Des Melanges D'Antipodes Optiques. VI.-Derives Du Dihydro-9,10 ethano-9,10-anthracene. *Bull. Soc. Chim. Fr.* **1973**, *1*, 190−197.
(33) Thunberg, L.; Allenmark, S. Asymmetric Cycloaddition Routest to Both Enantiomers of Trans-9,10-dihydro-9,10-ethanoanthracene-11,12-dicarboxylic Acid. *Tetrahedron: Asymmetry* **2003**, *14*, 1317−1322.
(34) Ramanathan, C. R.; Periasamy, M. Resolution of C_2-symmetric 9,10-dihydro-9,10-ethanoanthracene-11,12-dicarboxylic Acid and 2,3-diphenylsuccinic Acid Using (*S*)-proline. *Tetrahedron: Asymmetry* **1998**, *9*, 2651−2656.
(35) Hagishita, S.; Kuriyama, K. Optical Activity of C_2-symmetrical 9,10-dihydro-9,10-ethanoanthracenes. *Tetrahedron* **1972**, *28*, 1435−1467.
(36) Brienne, M.-J.; Jacques, J. Optically Active Ethanoanthracenes. *C. R. Acad. Sci. C* **1971**, *272*, 1889−1891.
(37) Amsterdam Density Functional Program. Theoretical Chemistry, Vrije Universiteit, Amsterdam, URL http://www.scm.com.
(38) Te Velde, G.; Bickelhaupt, F. M.; Baerends, E. J.; Fonseca Guerra, C.; Van Gisbergen, S. J. A.; Snijders, J. G.; Ziegler, T. Chemistry with ADF. *J. Comput. Chem.* **2001**, *22*, 931−967.
(39) Fonseca Guerra, C.; Snijders, J. G.; te Velde, G.; Baerends, E. J. Towards an Order-n DFT Method. *Theor. Chem. Acc.* **1998**, *99*, 391−403.
(40) Nicu, V. P.; Neugebauer, J.; Wolff, S. K.; Baerends, E. J. A Vibrational Circular Dichroism Implementation within a Slater-type-orbital Based Density Functional Framework and its Application to Hexa- and Hepta-helicenes. *Theor. Chem. Acc.* **2008**, *119* (1−3), 245−263.
(41) Perdew, J. P. Density-functional Approximation for the Correlation Energy of the Inhomogeneous Electron Gas. *Phys. Rev. B* **1986**, *33*, 8822−8824.
(42) Becke, A. D. Density-functional Exchange-energy Approximation with Correct Asymptotic Behavior. *Phys. Rev. A* **1988**, *38*, 3098−3100.
(43) van Lenthe, E.; Baerends, E. J. Optimized Slater-type Basis Sets for Elements 1−118. *J. Comput. Chem.* **2003**, *24*, 1142−1156.
(44) Klamt, A.; Schűrmann, G. Cosmo: A New Approach to Dielectric Screening in Solvents with Explicit Expressions for the Screening Energy and its Gradient. *J. Chem. Soc., Perkin Trans.* **1993**, *2*, 799−805.
(45) Klamt, A. Conductor-like Screening Model for Real Solvents: A New Approach to the Quantitative Calculation of Solvation Phenomena. *J. Phys. Chem.* **1995**, *99*, 2224−2235.
(46) Klamt, A.; Jones, V. Treatment of the Outlying Charge in Continuum Solvation Models. *J. Chem. Phys.* **1996**, *105*, 9972−9981.
(47) Nicu, V. P.; Debie, E.; Herrebout, W.; Van der Veken, B.; Baerends, E. J.; Bultinck, P. A. Robust Mode Analysis of Transfer of Chirality in VCD: The Case of Pulegone. *Chirality* **2010**, *21*, 5287−5297.
(48) Holzwarth, G.; Chabay, I. Optical Activity of Vibrational Transitions: Coupled Oscillator Model. *J. Chem. Phys.* **1972**, *57*, 1632−1635.
(49) Bouř, P.; Keiderling, T. A. Ab Initio Simulations of the Vibrational Circular Dichroism of Coupled Peptides. *J. Am. Chem. Soc.* **1993**, *115*, 9602−9607.
(50) Taniguchi, T.; Monde, K. The Exciton Chirality Method in Vibrational Circular Dichroism. *J. Am. Chem. Soc.* **2012**, *134*, 3695−3698.
(51) Setnicka, V.; Urbanova, M.; Bouř, P.; Kral, V.; Volka, K. Vibrational Circular Dichroism of 1,1-binaphthyl Derivatives: Experimental and Theoretical Study. *J. Phys. Chem. A* **2001**, *105*, 8931−8938.
(52) Abbate, S.; Burgi, L. F.; Castiglioni, E.; Lebon, F.; Longhi, G.; Toscano, F.; Caccamese, S. Assessment of Configurational and Conformational Properties of Naringenin by Vibratioanl Circular Dichroism. *Chirality* **2009**, *21*, 436−441.
(53) Abbate, S.; Lebon, F.; Gangemi, R.; Longhi, G.; Spizzichino, S.; Ruzziconi, R. Electronic and Vibrational Circular Dichroism Spectra of Chiral 4-X-[[2.2]paracyclophanes with X Containing Fluorine Atoms. *J. Phys. Chem. A* **2009**, *113*, 14851−14859.
(54) Liegeois, V. A Vibrational Raman Optical Activity Study of 1,1′-binaphthyl Derivatives. *ChemPhysChem* **2009**, *10*, 2017−2025.
(55) Merten, C.; Amkreutz, M. V.; Hartwig, A. Determining the Structure of Alpha-phenylethyl Isocyanide in Chloroform by VCD

748 Spectroscopy and DFT Calculations. Simple Case or Challenge? *Phys.*
749 *Chem. Chem. Phys.* **2010**, *12*, 11635−11641.
750 (56) Banks, S. T.; Clary, D. C. Chemical Reaction Surface Vibrational
751 Frequencies Evaluated in Curvilinear Internal Coordinates: Applica-
752 tion to $H+CH_4 \leq > H_2+CH_3$. *J. Chem. Phys.* **2009**, *130*, 024106.
753 (57) Longhi, G.; Zerbi, G.; Paterlini, G.; Ricard, L.; Abbate, S.
754 Conformational Dependence of CH(CD)-Stretchings in D-Glucose
755 and Some Deuterated Derivatives as Revealed by Infrared and Raman
756 Spectroscopy. *Carbohydr. Res.* **1987**, *161*, 1−22.
757 (58) Lewis, B. E.; Schramm, V. L. Conformational Equilibrium
758 Isotope Effects in Glucose by C13-NMR Spectroscopy and Computa-
759 tional Studies. *J. Am. Chem. Soc.* **2001**, *123*, 1327−1336.